NASA Technical Memorandum 81850

A Potential-Flow/Boundary-Layer Method for Calculating Subsonic and Transonic Airfoil Flow With Trailing-Edge Separation

Richard W. Barnwell

JUNE 1981

NASA

NASA Technical Memorandum 81850

A Potential-Flow/Boundary-Layer Method for Calculating Subsonic and Transonic Airfoil Flow With Trailing-Edge Separation

Richard W. Barnwell
Langley Research Center
Hampton, Virginia

National Aeronautics
and Space Administration

**Scientific and Technical
Information Branch**

1981

SUMMARY

The development of a potential-flow/boundary-layer method for calculating subsonic and transonic turbulent flow past airfoils with trailing-edge separation is reported. A moment-of-momentum integral boundary-layer method is used which employs the law-of-the-wall/law-of-the-wake velocity profile and a two-layer eddy-viscosity model and ignores the laminar sublayer. All integrals across the boundary layer are obtained in closed form. Separation is assumed to occur when the shearing-stress velocity vanishes. A closed-form solution is derived for separated-flow regions where the shearing stress is negligible. In the potential-flow method, the exact form of the airfoil boundary condition is used, but it is applied at the chord line rather than at the airfoil surface. This allows the accurate computation of flow about airfoils at large angles of attack but permits the use of body-oriented Cartesian computational grids. The governing equation for the perturbation velocity potential contains several terms in addition to the classical small-disturbance terms.

INTRODUCTION

This paper reports on the development of a potential-flow/boundary-layer method for calculating two-dimensional subsonic and transonic separated flow past airfoils. The form of separation which is discussed is the turbulent trailing-edge type. Previous potential-flow/boundary-layer treatments of the trailing-edge separation problem (refs. 1 to 6, for example) have been restricted to low-speed flow. Previous treatments of the transonic trailing-edge separation problem (ref. 7, for example) have used solutions to the Navier-Stokes equations, which are very expensive to compute.

The present method was developed to show that it is possible and feasible to calculate separated flow past relatively thick, cambered airfoils with angles of attack near stall and fairly large subsonic free-stream Mach numbers up to the drag-divergence Mach number. These are the conditions under which many rotorcraft and aircraft airfoils operate. It is not the intent at this time to discuss leading-edge separation or shock-induced separation (separation at the shock wave). The basic conclusion of the present report is that it is, in fact, possible and feasible to calculate transonic flow past airfoils having trailing-edge separation with a potential-flow/boundary-layer method.

The boundary-layer and the potential-flow methods which are used are described in the next two sections. The methods are coupled in that the boundary-layer method uses edge-velocity distributions computed from the potential-flow program, and the potential-flow program uses a displacement thickness and a separation-point location determined by the boundary-layer method.

SYMBOLS

A,B,C	coefficients of potential-flow governing equation
a	speed of sound
a_{ij},b_i,c_i	coefficients of boundary-layer equations ($i = 1,2,3$ and $j = 1,2,3$)
$\tilde{B}$	law-of-the-wall boundary-layer coefficient
C_l	lift coefficient
C_p	pressure coefficient
$C_p{}^*$	sonic pressure coefficient
c	airfoil chord
$c_3{}^*,\tilde{c}_3$	normalized forms of c_3 for $u^* = 0$
d_i	coefficients in equation for gradient of displacement thickness ($i = 1,2,3,4$)
$I_1,\ldots,I_5$	definite integrals
K	coefficient in Clauser model for eddy viscosity
M	Mach number
p	pressure
R_θ	transition point Reynolds number based on momentum thickness
S	Sutherland temperature parameter
U,W	transformed velocity components
u,w	x and z velocity components
$u^*,u\beta$	law-of-the-wall and law-of-the-wake velocity parameters
v	perturbation velocity parameter
v_∞	free-stream speed
x,z	Cartesian coordinates for chordwise and normal directions in inviscid treatment and for tangential and normal directions in boundary-layer treatment
α	angle of attack

β	edge-velocity gradient parameter
Γ	circulation
γ	ratio of specific heats
$\tilde{\gamma}$	intermittency factor
Δa_{33}	increment added to a_{33}
Δc_3	increment added to c_3
$\Delta x, \Delta z$	mesh spacings in x and z directions
δ	boundary-layer thickness in transform plane (distance from surface at which $U = U_e$)
δ_c	boundary-layer thickness parameter in physical plane
δ^*	boundary-layer displacement thickness
ε	eddy viscosity
ε_i	eddy viscosity in inner layer
ε_o	eddy viscosity in outer layer
η, ξ	normal and tangential boundary-layer coordinates in transform plane
η_j	value of η where $U = 0$
θ	boundary-layer momentum thickness
κ	law-of-the-wall boundary-layer coefficient
μ_t	turbulent viscosity
ν	kinematic viscosity
Π	coefficient used in starting solution to relate u^* and u_β
ρ	density
ρ_w	density at wall
Φ	single-variable velocity potential in transformed plane
φ	single-variable velocity potential in physical plane
ϕ	perturbation-velocity potential

Subscripts:

e	boundary-layer edge
i	interface between inner and outer layers of boundary layer
s	separation point
te	trailing edge
∞	free stream
$\pm$	upper and lower surfaces of airfoil

INTEGRAL BOUNDARY-LAYER METHOD FOR TURBULENT FLOW

Derivation of Equations

The present boundary-layer method is a simplified form of the turbulent-flow integral method of Kuhn and Nielsen (ref. 8), which is a refinement of the method of Nash and Hicks (ref. 9). The equations which are solved are the momentum equation, the moment-of-momentum equation, and a boundary-layer edge condition. The present model, like the model of reference 9, does not include the laminar sublayer. The wall is assumed to be adiabatic and the turbulent Prandtl number to be 1 so that the total enthalpy is constant across the boundary layer. The Reynolds stress is approximated with an eddy-viscosity model which is like the Cebeci-Smith model (ref. 10) but does not contain laminar-sublayer terms. Compressibility is accounted for with the Stewartson transformation (ref. 11) as in reference 8.

The fact that the laminar sublayer can be ignored in the present integral treatment of separated flow may appear unusual to researchers acquainted with finite-difference solutions to the boundary-layer and Navier-Stokes equations. The influence of the sublayer on the physical solution diminishes as separation is approached because the sublayer thickness decreases whereas the boundary-layer, displacement, and momentum thicknesses increase rapidly. As a result, the physical error incurred by neglecting the laminar sublayer at separation is actually less than that incurred in the attached-flow region. However, for finite-difference treatments of the separation problem, the influence of the sublayer on the numerical solution increases drastically because some minimum number of grid points must be maintained within the shrinking sublayer at the same time that the boundary layer as a whole is increasing rapidly in thickness. Thus, in finite-difference solutions of the separation problem, resolution must be increased in a region of diminishing physical importance at the same time that higher resolution is needed for physical reasons in other parts of the solution domain.

The continuity, momentum, and energy equations which govern the turbulent compressible flow under consideration are

$$\frac{\partial(\rho u)}{\partial x} + \frac{\partial(\rho w)}{\partial z} = 0 \tag{1}$$

$$\rho u \frac{\partial u}{\partial x} + \rho w \frac{\partial u}{\partial z} = - \frac{\partial p}{\partial x} + \frac{\partial}{\partial z}\left(\mu_t \frac{\partial u}{\partial z}\right) \tag{2}$$

and

$$\frac{\gamma}{(\gamma - 1)} \frac{p}{\rho} + \frac{1}{2}(u^2 + w^2) = \frac{\gamma}{(\gamma - 1)} \frac{p_\infty}{\rho_\infty} + \frac{1}{2} v_\infty^2 \tag{3}$$

where x and z are the tangential and normal coordinates, u and w are the respective velocity components, p, ρ, and γ are the pressure, the density, and the ratio of specific heats, and μ_t is the turbulent viscosity. The pressure, density, and speed in the free stream are designated as p_∞, ρ_∞, and v_∞.

The transformed coordinates for the present version of the Stewartson transformation are

$$\xi = \int \frac{a_e}{a_\infty} dx \tag{4}$$

and

$$\eta = \frac{a_e}{a_\infty} \int \frac{\rho}{\rho_\infty} dz \tag{5}$$

where a is the speed of sound and the subscript e designates boundary-layer edge conditions. The transformed velocity components U and W are

$$U = \frac{a_\infty}{a_e} u \tag{6}$$

and

$$W = \frac{a_\infty^2}{a_e^2} \frac{\partial \eta}{\partial x} u + \frac{\rho}{\rho_\infty} \frac{a_\infty}{a_e} w \tag{7}$$

The governing partial differential equations are written in transform variables as

$$\frac{\partial U}{\partial \xi} + \frac{\partial W}{\partial \eta} = 0 \tag{8}$$

and

$$U \frac{\partial U}{\partial \xi} + W \frac{\partial U}{\partial \eta} = U_e \frac{dU_e}{d\xi} + \frac{\partial}{\partial \eta}\left(\frac{\rho^2}{\rho_\infty^2} \varepsilon \frac{\partial U}{\partial \eta}\right) \tag{9}$$

where

$$\varepsilon = \frac{\mu_t}{\rho} \tag{10}$$

is the eddy viscosity.

Coles' law-of-the-wall/law-of-the-wake velocity profile (ref. 12), which is used in the present method, can be written as

$$U = u^*\left[\frac{1}{\kappa} \ln\left(\frac{\eta u^*}{\nu_\infty}\right) + \tilde{B}\right] + u_\beta \sin^2\left(\frac{\pi}{2} \frac{\eta}{\delta}\right) \tag{11}$$

where δ is the boundary-layer thickness (distance from the wall at which $U = U_e$), u^* and u_β are the wall and wake velocity parameters, ν_∞ is the free-stream kinematic viscosity, and κ and $\tilde{B}$ are constants which are given the values 0.41 and 5.00, respectively, in this report. Note that at the boundary-layer edge, equation (11) has the form

$$U_e = u^*\left[\frac{1}{\kappa} \ln\left(\frac{\delta u^*}{\nu_\infty}\right) + \tilde{B}\right] + u_\beta \tag{12}$$

and that the derivative of equation (12) with respect to ξ can be written as

$$a_{11}\frac{du^*}{d\xi} + a_{12}\frac{du_\beta}{d\xi} + a_{13}\frac{d\delta}{d\xi} = b_1\frac{dU_e}{d\xi} \tag{13}$$

where

$$a_{11} = \delta\left(U_e - u_\beta + \frac{u^*}{\kappa}\right) \tag{14}$$

$$a_{12} = b_1 = u^*\delta \tag{15}$$

$$a_{13} = \frac{u^{*2}}{\kappa} \tag{16}$$

Note also that the boundary-layer displacement thickness δ^* and momentum thickness θ can be written as

$$\delta^* = \int_{z=0}^{z=\delta_c}\left(1 - \frac{\rho u}{\rho_e u_e}\right)dz = \frac{\rho_\infty a_\infty}{\rho_e a_e}\,\delta\left\{\left[\frac{u^*}{\kappa U_e} + \frac{u_\beta}{2U_e}\right]\left[1 + (\gamma - 1)M_e^2\right]\right.$$

$$\left. - \frac{\gamma - 1}{2}M_e^2\left[\frac{2u^{*2}}{\kappa^2 U_e^2} + \frac{3u_\beta^2}{8U_e^2} + \frac{(1 + I_1)(u^*u_\beta)}{\kappa U_e^2}\right]\right\} \tag{17}$$

and

$$\theta = \int_{z=0}^{z=\delta_c}\frac{\rho u}{\rho_e u_e}\left(1 - \frac{u}{u_e}\right)dz = \frac{\rho_\infty a_\infty}{\rho_e a_e}\,\delta\left\{\frac{u^*}{\kappa U_e} + \frac{u_\beta}{2U_e}\right.$$

$$\left. - \left[\frac{2u^{*2}}{\kappa^2 U_e^2} + \frac{3u_\beta^2}{8U_e^2} + \frac{(1 + I_1)(u^*u_\beta)}{\kappa U_e^2}\right]\right\} \tag{18}$$

where δ_c is the transformed value of δ in the physical plane, M is the Mach number, and the definite integral I_1 is

$$I_1 = \frac{1}{\pi} \int_{\sigma=0}^{\sigma=\pi} \frac{\sin \sigma}{\sigma} \, d\sigma = 0.58949 \tag{19}$$

The factor $\rho_\infty a_\infty / \rho_e a_e$ can be evaluated with the equation

$$\frac{\rho_\infty a_\infty}{\rho_e a_e} = \left[\frac{1 + \left(\frac{\gamma - 1}{2} \right) M_e^2}{1 + \left(\frac{\gamma - 1}{2} \right) M_\infty^2} \right]^{(\gamma+1)/2(\gamma-1)} \tag{20}$$

A two-layer eddy-viscosity model is used which is similar to the Cebeci-Smith model (ref. 10) but which does not have viscous sublayer terms. In the inner layer a Prandtl mixing-length model of the form

$$\varepsilon = \varepsilon_i = \kappa^2 z^2 \left| \frac{\partial u}{\partial z} \right| \cong \kappa^2 \eta^2 \left(\frac{\rho_\infty}{\rho} \right) \left| \frac{\partial U}{\partial \eta} \right| \tag{21}$$

is used. In the outer layer the Clauser model, which can be written as

$$\varepsilon = \varepsilon_o = K u_e \delta^* \tilde{\gamma} = K \left(\frac{a_e}{a_\infty} \right) U_e \delta^* \tilde{\gamma} \tag{22}$$

is employed, where K is a constant which, in the present method, is given the usual value of 0.016, and $\tilde{\gamma}$ is the intermittency factor.

In this report the intermittency factor is approximated with two line segments as

$$\left.\begin{aligned} \tilde{\gamma} &= 1 && \left(\eta \leq \frac{3}{5} \delta \right) \\ \tilde{\gamma} &= \frac{5}{2} \left(1 - \frac{\eta}{\delta} \right) && \left(\eta \geq \frac{3}{5} \delta \right) \end{aligned}\right\} \tag{23}$$

This simple approximation is compared with the experimental data of Klebanoff (ref. 13) and with the more elaborate empirical expressions of Klebanoff and of Cebeci-Smith (ref. 10) in figure 1.

As in most two-layer models, the switch from the inner to the outer-layer form is made at the point where the values of two forms are equal, that is,

$$\varepsilon_i = \varepsilon_o \tag{24}$$

In general, this point is located in the interior of the boundary layer where the intermittency factor is 1 and the density is approximately equal to the edge value. With equations (11), (21), and (22), equation (24) can be written as

$$\frac{\pi u \beta}{2U_e}\left(\frac{\eta_i}{\delta}\right)^2 \sin\left(\frac{\pi\eta_i}{\delta}\right) + \frac{u^*\eta_i}{\kappa U_e \delta} = \frac{\rho_e a_e}{\rho_\infty a_\infty}\frac{\kappa\delta^*}{\kappa\delta} \tag{25}$$

where η_i is the outer limit of the inner layer.

In the present method the differential equations which are solved are the integral forms of the momentum equation and the moment-of-momentum equation. With equations (8) and (11) the integral form of equation (9), the momentum equation, can be written as

$$-\int_{\eta=0}^{\eta=\delta}\left[U\frac{\partial U}{\partial \xi} + W\frac{\partial U}{\partial \eta} - U_e\frac{dU_e}{d\xi} - \frac{\partial}{\partial \eta}\left(\frac{\rho^2}{\rho_\infty{}^2}\,\varepsilon\frac{\partial U}{\partial \eta}\right)\right] d\eta$$

$$= a_{21}\frac{du^*}{d\xi} + a_{22}\frac{du\beta}{d\xi} + a_{23}\frac{d\delta}{d\xi} - b_2\frac{dU_e}{d\xi} - c_2 = 0 \tag{26}$$

where

$$a_{21} = \frac{\delta}{\kappa}\left[U_e - \frac{4}{\kappa}u^* - (1 + I_1)u\beta\right] \tag{27}$$

$$a_{22} = \frac{\delta}{2}\left[U_e - 2\frac{(1 + I_1)}{\kappa}u^* - \frac{3}{2}u\beta\right] \tag{28}$$

$$a_{23} = U_e\left(\frac{u^*}{\kappa} + \frac{u\beta}{2}\right) - \left[\frac{2}{\kappa^2}\,u^{*2} + \frac{(1 + I_1)}{\kappa}\,u^*u\beta + \frac{3}{8}\,u\beta^2\right] \tag{29}$$

$$b_2 = -2\delta\left(\frac{u^*}{\kappa} + \frac{u\beta}{2}\right) \tag{30}$$

$$c_2 = \frac{\rho_w}{\rho_\infty}\,u^*|u^*| \tag{31}$$

where ρ_w is the density at the wall. The ratio ρ_w/ρ_∞ is given by the equation

$$\frac{\rho_w}{\rho_\infty} = \frac{\left[1 + \frac{(\gamma - 1)}{2}\,M_\infty{}^2\right]^{1/(\gamma-1)}}{\left[1 + \frac{(\gamma - 1)}{2}\,M_e{}^2\right]^{\gamma/(\gamma-1)}} \tag{32}$$

Similarly, the moment-of-momentum equation can be written as

$$-\frac{1}{\delta}\int_{\eta=0}^{\eta=\delta}\eta\left[U\frac{\partial U}{\partial \xi} + W\frac{\partial U}{\partial \eta} - U_e\frac{dU_e}{d\xi} - \frac{\partial}{\partial \eta}\left(\frac{\rho^2}{\rho_\infty{}^2}\,\varepsilon\frac{\partial U}{\partial \eta}\right)\right]d\eta$$

$$= a_{31}\frac{du^*}{d\xi} + a_{32}\frac{du\beta}{d\xi} + a_{33}\frac{d\delta}{d\xi} - b_3\frac{dU_e}{d\xi} - c_3 = 0 \tag{33}$$

where

$$a_{31} = \frac{\delta}{\kappa}\left[\frac{U_e}{4} - \frac{u^*}{\kappa} - \left(\frac{5}{8} + \frac{2}{\pi^2} + \frac{3}{2}\,I_2\right)u\beta\right] \tag{34}$$

$$a_{32} = \delta\left[\left(\frac{1}{4} - \frac{1}{\pi^2}\right)U_e - \left(\frac{3}{8} + \frac{2}{\pi^2} + \frac{I_2}{2}\right)\frac{u^*}{\kappa} - \left(\frac{1}{2} - \frac{2}{\pi^2}\right)u_\beta\right] \tag{35}$$

$$a_{33} = \left(\frac{1}{2} - \frac{2}{\pi^2}\right)U_e u_\beta + \frac{u^* U_e}{2\kappa} - \frac{3u^{*2}}{4\kappa^2} - \frac{1}{\kappa}\left(\frac{3}{4} + \frac{2}{\pi^2} + I_2\right)u^* u_\beta - \left(\frac{5}{16} - \frac{1}{\pi^2}\right)u_\beta^2 \tag{36}$$

$$b_3 = -\delta\left[\frac{3u^*}{4\kappa} + \left(\frac{3}{4} - \frac{3}{\pi^2}\right)u_\beta\right] \tag{37}$$

$$c_3 = \frac{\kappa^2}{\delta}\int_{\eta=0}^{\eta=\eta_i} \eta^2 \frac{\rho}{\rho_\infty}\left|\frac{\partial u}{\partial \eta}\right|\frac{\partial u}{\partial \eta}\,d\eta + KU_e\frac{\delta^* a_e}{\delta a_\infty}\int_{\eta=\eta_i}^{\eta=\delta}\frac{\rho^2}{\rho_\infty^2}\tilde{\gamma}\frac{\partial u}{\partial \eta}\,d\eta \tag{38}$$

and where the definite integral I_2 is

$$I_2 = -\int_{\sigma=0}^{\sigma=\pi}\frac{1 - \cos\sigma}{\sigma}\,d\sigma = -0.16701 \tag{39}$$

The treatment of the shearing-stress integral in the term c_3 is one of the distinguishing features between the present method and the preceding methods of Kuhn and Nielsen (ref. 8) and Nash and Hicks (ref. 9). In reference 9 the term was approximated as a perturbation about the value for equilibrium flow. In reference 8 the integrals across the boundary layer were evaluated numerically because of the complexity caused by the inclusion of the laminar sublayer terms. In the present method the shearing-stress integral is integrated in closed form.

An additional approximation is made in order to evaluate the integrals in equation (38). The ratio ρ/ρ_∞ is

$$\frac{\rho}{\rho_\infty} = \frac{\rho_e/\rho_\infty}{1 + \frac{(\gamma - 1)M_\infty^2}{2v_\infty^2}\left(U_e^2 - U^2\right)} \tag{40}$$

In the present method it is assumed that for subsonic and transonic Mach numbers the ratios ρ/ρ_∞ and ρ^2/ρ_∞^2 can be approximated as

$$\frac{\rho}{\rho_\infty} \cong \frac{\rho_e}{\rho_\infty}\left[1 - \frac{(\gamma - 1)M_\infty^2}{2v_\infty^2}\left(U_e^2 - U^2\right)\right] \tag{41}$$

and

$$\frac{\rho^2}{\rho_\infty^2} \cong \left(\frac{\rho_e}{\rho_\infty}\right)^2\left[1 - (\gamma - 1)\frac{M_\infty^2}{v_\infty^2}\left(U_e^2 - U^2\right)\right] \tag{42}$$

With equations (11), (23), (41), and (42), the term c_3 in equation (38) is

$$\begin{aligned} c_3 = \frac{\rho_e}{\rho_\infty}\Bigg\{ & \frac{\eta_i}{\delta}\,u^{*2} + \frac{\kappa}{\pi}\left[\sin\left(\frac{\pi\eta_i}{\delta}\right) - \frac{\pi\eta_i}{\delta}\cos\left(\frac{\pi\eta_i}{\delta}\right)\right]u^* u_\beta \\ & + \kappa^2\left[\frac{\pi^2}{24}\left(\frac{\eta_i}{\delta}\right)^3 - \frac{\pi}{16}\left(\frac{\eta_i}{\delta}\right)^2\sin\left(\frac{2\pi\eta_i}{\delta}\right) - \frac{\eta_i}{16\delta}\cos\left(\frac{2\pi\eta_i}{\delta}\right)\right. \\ & \left. + \frac{1}{32\pi}\sin\left(\frac{2\pi\eta_i}{\delta}\right)\right]u_\beta^2 + \frac{(\gamma - 1)M_\infty^2\eta_i}{2v_\infty^2\delta}\,u^{*2}\left[\left(U_i - \frac{u^*}{\kappa}\right)^2 + \frac{u^{*2}}{\kappa^2} - U_e^2\right]\Bigg\} \\ & + \frac{a_e\rho_e^2}{a_\infty\rho_\infty^2}\,KU_e\,\frac{\delta^*}{\delta}\Bigg\{\left[\frac{3}{2}\ln\left(\frac{5}{3}\right) - 1 - \ln\left(\frac{\eta_i}{\delta}\right)\right]\frac{u^*}{\kappa} \\ & + \left[\frac{1}{2}\cos\left(\frac{\pi\eta_i}{\delta}\right) + \frac{5}{4\pi}\sin\left(\frac{3\pi}{5}\right)\right]u_\beta + (\gamma - 1)\frac{M_\infty^2}{v_\infty^2}\left(U_e^2 U_i - \frac{1}{3}U_i^3 - \frac{2}{3}U_e^3\right)\Bigg\} \end{aligned} \tag{43}$$

where U_i is the value of U at the point $\eta = \eta_i$. In regions where the flow is separated the term

$$\Delta c_3 = -2 \frac{\rho_e}{\rho_\infty} \left\{ \left[1 - \frac{(\gamma - 1)}{2} M_e^2 \right] \frac{\eta_j}{\delta} u^{*2} + \frac{\kappa}{\pi} \left[\sin\left(\frac{\pi\eta_j}{\delta}\right) - \frac{\pi\eta_j}{\delta} \cos\left(\frac{\pi\eta_j}{\delta}\right) \right] u^* u_\beta \right.$$

$$+ \kappa^2 \left[\frac{\pi^2}{24}\left(\frac{\eta_j}{\delta}\right)^3 - \frac{\pi}{16}\left(\frac{\eta_j}{\delta}\right)^2 \sin\left(\frac{2\pi\eta_j}{\delta}\right) - \frac{\eta_j}{16\delta} \cos\left(\frac{2\pi\eta_j}{\delta}\right) \right.$$

$$\left. \left. + \frac{1}{32\pi} \sin\left(\frac{\pi\eta_j}{\delta}\right) \right] u_\beta^2 \right\} \tag{44}$$

must be added to equation (43) to account for the absolute value in the first term on the right side of equation (38). The point at which U vanishes is designated η_j. It has been assumed that η_j is less than η_i.

The quantities ξ and U_e are more difficult to deal with than x and u_e. Therefore, equations (13), (26), and (33) are transformed into

$$a_{i1} \frac{du^*}{dx} + a_{i2} \frac{du_\beta}{dx} + a_{i3} \frac{d\delta}{dx} = b_i \frac{dU_e}{du_e} \frac{du_e}{dx} + \frac{a_e}{a_\infty} c_i \qquad (i = 1,2,3) \tag{45}$$

for purposes of numerical integration. The quantities U_e, M_e, dU_e/du_e, and a_e/a_∞ are given by the following equations:

$$U_e = \frac{u_e}{\sqrt{1 + \frac{(\gamma - 1)}{2} M_\infty^2 (1 - u_e^2/v_\infty^2)}} \tag{46}$$

$$M_e = \frac{U_e}{v_\infty} M_\infty \tag{47}$$

$$\frac{dU_e}{du_e} = \frac{1 + \frac{(\gamma - 1)}{2} M_\infty^2}{\left[1 + \frac{(\gamma - 1)}{2} M_\infty^2 \left(1 - u_e^2/v_\infty^2\right)\right]^{3/2}} \tag{48}$$

and

$$\frac{a_e}{a_\infty} = \sqrt{\frac{1 + \frac{(\gamma - 1)}{2} M_\infty^2}{1 + \frac{(\gamma - 1)}{2} M_e^2}} \tag{49}$$

If $|a_{ij}|$, the determinant of the coefficient matrix for equations (45), vanishes, the derivatives du^*/dx, du_β/dx, and $d\delta/dx$ become unbounded. This type of behavior is expected for a direct boundary-layer solution at a separation point, but it is not expected before separation occurs. However, because of the approximate nature of the present treatment, the determinant for the present method vanishes at a point just upstream of separation as well as at the separation point. In order to improve the behavior of the numerical solution, the moment-of-momentum equation is manipulated so that the resulting coefficient matrix does not vanish until the separation point is reached. The manipulation consists of adding the quantities

$$\Delta a_{33} = - \frac{\frac{1}{2}\left(\frac{1}{8} - \frac{1}{\pi^2}\right) + \left[\frac{3}{4}\left(\frac{1}{4} - I_1 + I_2\right) + \frac{4}{\pi^2}\left(\frac{1}{4} + I_1\right)\right]\frac{a_{12}}{\kappa a_{11}}}{1 - 4I_1 \frac{a_{12}}{\kappa a_{11}}} u_\beta^2 \tag{50}$$

and

$$\Delta c_3 = \Delta a_{33} \frac{d\delta}{dx} \tag{51}$$

to equations (36) and (43). The effect of this manipulation is to lag the solution for the derivative $d\delta/dx$.

Starting Solution

In order to start the numerical integration of the boundary-layer equations it is necessary to obtain the initial solution for u^*, u_β, and δ at the transition point. This solution is determined by iterative solution of equations (12), (18), and the equation

$$u_\beta = \frac{2}{\kappa} \Pi u^* \tag{52}$$

for a specified value of the transition-point Reynolds number based on momentum thickness R_θ. An expression for the quantity Π is obtained from reference 14 as

$$\Pi = \frac{4}{5}\left(\beta + \frac{1}{2}\right)^{3/4} \tag{53}$$

where

$$\beta = -\frac{\rho_e u_e \delta^*}{\rho_w u^{*2}} \frac{du_e}{dx} \tag{54}$$

The momentum thickness is related to the Reynolds number based on momentum thickness by the equation

$$\theta = \nu_e R_\theta / u_e \tag{55}$$

where

$$\nu_e = \frac{\nu_\infty \left(\frac{T_\infty + S}{T_e + S}\right)}{\left(\frac{T_e}{T_\infty}\right)^{(5-3\gamma)/2(\gamma-1)}} \tag{56}$$

where T_∞ and T_e are the free-stream and boundary-layer-edge temperatures, ν_∞ is the free-stream kinematic viscosity, and S is the Southerland temperature parameter. The transition-point Reynolds number based on momentum thickness is generally given a value of 320.

Integration of Equations in Attached-Flow Region

The solution for the quantities u^*, u_β, and δ is advanced downstream in the attached-flow region by numerical integration of equations (45). A second-order predictor-corrector technique is used in the integration process. The edge velocity u_e and the gradient of the edge velocity are obtained from the current inviscid solution. The numerical integration is terminated at the separation point, where u^* vanishes.

It it interesting to note that the differential equations do not depend explicitly on the kinematic viscosity. Therefore, the Reynolds number influences only the starting solution explicitly. This result is a consequence of ignoring the laminar sublayer.

In the present method there are two options for evaluating the law-of-the-wake velocity parameter u_β. The most obvious procedure is to use the value obtained from the integration of equations (45). The second procedure is to use equation (12), which is the integrated form of the first of equations (45). The second procedure reduces errors incurred in numerical integration which tend to be disruptive as the separation point is approached and the determinant of the coefficient matrix $|a_{ij}|$ approaches zero. Another advantage to the use of equation (12) is that it makes the solution explicitly dependent on the kinematic viscosity and hence the Reynolds number.

In regions where the inviscid flow is expanding, the parameter u_β approaches zero but should not become negative. If the numerical procedure discussed previously predicts a negative value for u_β, the quantities u_β and du_β/dx in the second and third of equations (45) are given values of zero, and these equations are solved for du^*/dx and $d\delta/dx$ and hence for u^* and δ.

Integration of Equations in Separated-Flow Region

It has been pointed out in references 8 and 9 that numerical solutions to boundary-layer equations posed in the form of equations (45) are not stable in regions of separated flow. However, stable solutions can be obtained if the law-of-the-wall velocity parameter u^* is prescribed and equations (45) are solved for the quantities u_β, δ, and u_e (or U_e).

The present method is intended for use in treating flow about airfoils with trailing-edge separation. It is well-known empirically that the reverse-flow speed is small relative to free-stream speed in most trailing-edge separated flows. Therefore, it is assumed in the present method that u^* is zero in separated-flow regions. It follows from the first of equations (45) that du^*/dx is also zero in these regions. It is also assumed in the present method that the entire region from the first separation point detected to the trailing edge is separated.

When u^* and du^*/dx are zero, the quantities u_β and du_β/dx are equal to U_e and dU_e/dx, and the second and third of equations (45) can be written as

$$\frac{1}{\delta}\frac{d\delta}{dx} + \frac{6}{U_e}\frac{dU_e}{dx} = 0 \tag{57}$$

and

$$\left(\frac{3}{16} - \frac{1}{\pi^2}\right)\frac{1}{\delta}\frac{d\delta}{dx} + 2\left(\frac{1}{4} - \frac{1}{\pi^2}\right)\frac{1}{U_e}\frac{dU_e}{dx} = \frac{\tilde{c}_3}{\delta} \tag{58}$$

where

$$\tilde{c}_3 = \left. \frac{a_e}{a_\infty} \frac{c_3}{U_e^2} \right|_{u^*=0} \tag{59}$$

The quantity $\tilde{c}_3$ depends only weakly on U_e and is considered constant in the present treatment.

There is a simultaneous closed-form solution to equations (57) and (58) which can be written as follows:

$$\delta = \delta_s [1 + c_3^*(x - x_s)] \tag{60}$$

and

$$U_e = \frac{U_{e,s}}{[1 + c_3^*(x - x_s)]^{1/6}} \tag{61}$$

where δ_s, $U_{e,s}$, and x_s are separation-point values and where

$$c_3^* = \frac{48\pi^2}{(5\pi^2 - 32)} \frac{\tilde{c}_3}{\delta_s} \tag{62}$$

The quantities δ_s and x_s are determined from the boundary-layer solution. However, the quantity $U_{e,s}$ is determined from the inviscid solution in order to couple the viscous and inviscid solutions and to facilitate convergence.

In order to derive an expression for $U_{e,s}$, a single-variable velocity-potential function Φ is introduced which is related to the edge velocity in the transformed plane U_e by the following equation:

$$U_e = \frac{d\Phi}{dx} \tag{63}$$

With equation (61), equation (63) can be integrated to determine the function Φ. The following equation for $U_{e,s}$ is obtained from this function evaluated at the trailing edge:

$$U_{e,s} = \frac{5}{6} \frac{c_3^*(\Phi_{te} - \Phi_s)}{[1 + c_3^*(x_{te} - x_s)]^{5/6} - 1} \tag{64}$$

where Φ_s is the separation-point value and Φ_{te} and x_{te} are trailing-edge values. The value given by equation (64) and the value of U_e at the separation point converge as the inviscid solution converges.

In order to obtain the solution for the edge velocity in the physical plane u_e, this quantity is associated with a single-variable velocity-potential function φ, and it is noted that U_e (and hence u_e) does not vary a great deal in separated-flow regions. It follows that

$$u_e = \frac{d\varphi}{dx} = \frac{d\varphi}{d\Phi} U_e \cong \frac{\varphi_{te} - \varphi_s}{\Phi_{te} - \Phi_s} U_e \tag{65}$$

or

$$u_e = \frac{5}{6} \frac{c_3^*(\varphi_{te} - \varphi_s)}{\left\{[1 + c_3^*(x_{te} - x_s)]^{5/6} - 1\right\}[1 + c_3^*(x - x_s)]^{1/6}} \tag{66}$$

The evaluation of the velocity potentials φ_{te} and φ_s is discussed in the section of the paper entitled "Approximate Potential-Flow Method." Equation (66) is used to evaluate the quantity u_e in equation (97) for the Dirichlet boundary conditions for the inviscid solution in the separated-flow region.

It has been found that equation (66) tends to overpredict the variation of u_e for incompressible and low-speed conditions for which it is well-known empirically that u_e is almost constant. Therefore, the present method contains an option to evaluate u_e in the limit as c_3^* vanishes. This value is

$$u_e = \frac{\varphi_{te} - \varphi_s}{x_{te} - x_s} \tag{67}$$

Evaluation of Displacement-Thickness Gradient

In the attached-flow region the inviscid solution is influenced by the boundary-layer solution through the quantity $d\delta^*/dx$, the gradient of the displacemnt thickness. It is common practice to determine δ^* from the boundary-layer solution and then obtain $d\delta^*/dx$ by numerical differentiation. In general, this procedure produces eratic variations of $d\delta^*/dx$ which must be smoothed.

In the present method the gradient $d\delta^*/dx$ is calculated directly from the gradients of u^*, u_β, δ, and u_e. The expression for this gradient, which is the derivative of equation (17) with respect to x, is

$$\frac{d\delta^*}{dx} = d_1 \frac{du^*}{dx} + d_2 \frac{du_\beta}{dx} + d_3 \frac{d\delta}{dx} + d_4 \frac{du_e}{dx} \tag{68}$$

where

$$d_1 = \frac{a_e \rho_e}{a_\infty \rho_\infty} \frac{\delta}{\kappa U_e} \left\{ 1 + (\gamma - 1) M_e^2 \left[1 - \frac{2}{\kappa} \frac{u^*}{U_e} - \frac{(1 + I_1) u_\beta}{2U_e} \right] \right\} \tag{69}$$

$$d_2 = \frac{a_e \rho_e}{a_\infty \rho_\infty} \frac{\delta}{2U_e} \left\{ 1 + (\gamma - 1) M_e^2 \left[1 - \frac{(1 + I_1) u^*}{\kappa U_e} - \frac{3u_\beta}{4U_e} \right] \right\} \tag{70}$$

$$d_3 = \frac{\delta^*}{\delta} \tag{71}$$

$$d_4 = \frac{dU_e}{du_e} \left\{ \frac{(\gamma + 1)}{2} \frac{M_\infty M_e}{1 + \frac{(\gamma - 1)}{2} M_e^2} \frac{\delta^*}{v_\infty} \right.$$

$$\left. - \frac{a_e \rho_e}{a_\infty \rho_\infty} \left[1 - (\gamma - 1) M_\infty^2 \right] \left[\frac{1}{\kappa} \frac{u^*}{U_e} + \frac{u_\beta}{2U_e} \right] \frac{\delta}{U_e} \right\} \tag{72}$$

It is not necessary to smooth the values obtained from equation (68) with respect to x. However, it is necessary to relax the values of $d\delta^*/dx$ with respect to the inviscid-solution iteration variable near the trailing edge. Equation (68) is used to evaluate the gradient $d\delta^*/dx$ in equations (95) and (96) for the Neumann boundary conditions for the inviscid solution in the attached-flow region.

Alternate Form of Third Equation

In the present treatment, as in that of Kuhn and Nielsen (ref. 8) and of Nash and Hicks (ref. 9), the third equation is the moment-of-momentum equation. An alternate approach involves the use of the integral mean kinetic-energy equation, which can be written as

$$- \frac{1}{\delta} \int_{\eta=0}^{\eta=\delta} U \left[U \frac{\partial U}{\partial \xi} + W \frac{\partial U}{\partial \eta} - U_e \frac{dU_e}{d\xi} - \frac{\partial}{\partial \eta} \left(\frac{\rho^2}{\rho_\infty{}^2} \varepsilon \frac{\partial U}{\partial \eta} \right) \right] d\eta$$

$$= a_{31} \frac{du^*}{d\xi} + a_{32} \frac{du_\beta}{d\xi} + a_{33} \frac{d\delta}{d\xi} - b_3 \frac{dU_e}{d\xi} - c_3 = 0 \tag{73}$$

where

$$a_{31} = - \frac{\delta}{\kappa} \left\{ U_e \left[\frac{2u^*}{\kappa} + \frac{(1 + I_1)}{2} u_\beta \right] + 3 \left(\frac{3u^{*2}}{\kappa^2} + I_3 \frac{u^* u_\beta}{\kappa} + \frac{I_4}{4} u_\beta{}^2 \right) \right\} \tag{74}$$

$$a_{32} = - \frac{\delta}{2} \left\{ U_e \left[(1 + I_1) \frac{u^*}{\kappa} + \frac{3}{4} u_\beta \right] + 3 \left(I_3 \frac{u^{*2}}{\kappa^2} + I_4 \frac{u^* u_\beta}{\kappa} + \frac{5}{16} u_\beta{}^2 \right) \right\} \tag{75}$$

$$a_{33} = - \frac{U_e}{2} \left[\frac{2u^{*2}}{\kappa^2} + (1 + I_1) \frac{u^* u_\beta}{\kappa} + \frac{3}{8} u_\beta{}^2 \right] + 3 \left(\frac{u^{*3}}{\kappa^3} + \frac{I_3}{2} \frac{u^{*2} u_\beta}{\kappa^2} \right.$$

$$\left. + \frac{I_4}{4} \frac{u^* u_\beta{}^2}{\kappa} + \frac{5}{96} u_\beta{}^3 \right) \tag{76}$$

$$b_3 = \frac{3\delta}{2} \left[\frac{2u^{*2}}{\kappa^2} + (1 + I_1) \frac{u^* u_\beta}{\kappa} + \frac{3}{8} u_\beta{}^2 \right] \tag{77}$$

$$c_3 = -\frac{\rho_w}{\rho_\infty} U_e u^* |u^*| + \kappa^2 \frac{\rho_e}{\rho_\infty} \left[\ln(\eta_i) \frac{u^{*3}}{\kappa^3} + \frac{3}{4} \pi^2 \eta_i^2 \left(1 - \frac{\pi^2 \eta_i^2}{12} + \frac{\pi^4 \eta_i^4}{360} \right) \frac{u^{*2} u_\beta}{\kappa} \right.$$

$$\left. + \frac{3}{16} \pi^4 \eta_i^4 \left(1 - \frac{2}{9} \pi^2 \eta_i^2 \right) \frac{u^* u_\beta^2}{\kappa} + \frac{\pi^6 \eta_i^6}{48} u_\beta^3 + (U_e - U_\beta) \frac{u^{*2}}{\kappa^2} \right]$$

$$+ \frac{(\gamma - 1)}{2} M_\infty^2 \kappa^2 \frac{\rho_e}{\rho_\infty} \frac{u^{*2}}{\kappa^2} \left[\ln(\eta_i)(u_\beta - 2U_e) \frac{u^* u_\beta}{\kappa} + \ln^2(\eta_i)(U_e - u_\beta) \frac{u^{*2}}{\kappa^2} \right.$$

$$\left. + \frac{1}{3} \ln^3(\eta_i) \frac{u^{*3}}{\kappa^3} - \frac{1}{3}(U_e - u_\beta)(2U_e^2 + 2u_\beta U_e - u_\beta^2) \right]$$

$$+ K \frac{a_e \rho_e^2}{a_\infty \rho_\infty^2} \frac{\delta^*}{\delta} U_e \left(\left[\frac{1}{\eta_i} - \frac{5}{2} \ln\left(\frac{5}{3}\right) \right] \frac{u^{*2}}{\kappa^2} + \left[I_5 - 5 \sin^2\left(\frac{\pi}{5}\right) \right.\right.$$

$$\left. - \pi^2 \eta_i \left(1 - \frac{\pi^2 \eta_i^2}{18} \right) \right] \frac{u^* u_\beta}{\kappa} + \frac{\pi^2}{8} \left\{ \frac{4}{5} - \eta_i + \frac{5}{8\pi^2} \left[1 + \cos\left(\frac{\pi}{5}\right) \right] \right.$$

$$\left.\left. + \frac{1}{2\pi} \sin(2\pi\eta_i) \right\} u_\beta^2 \right) \tag{78}$$

The definite integrals I_3, I_4, and I_5 are given in the following equations:

$$I_3 = 1 + \frac{1}{2\pi} \int_{\sigma=0}^{\sigma=\pi} \ln^2(\sigma/\pi) \cos\sigma \, d\sigma = 1.16713 \tag{79}$$

$$I_4 = \frac{3}{4} + I_1 + \frac{1}{8\pi} \int_{\sigma=0}^{\sigma=\pi} \frac{\sin(2\sigma)}{\sigma} d\sigma = 1.39592 \tag{80}$$

$$I_5 = \pi^2 \left[\frac{5}{2} I_1 - \frac{3}{2\pi} \int_{\sigma=0}^{\sigma=\pi} \frac{\sin(3\sigma/5)}{\sigma} d\sigma \right] = 7.23979 \tag{81}$$

In the regions where the flow is reversed, the following quantity is added to equation (78):

$$\Delta c_3 = -2\kappa^2 \frac{\rho_e}{\rho_\infty}\left[\ln(\eta_j)\frac{u^{*3}}{\kappa^3} + \frac{3}{4}\pi^2\eta_j^2\left(1 + \frac{\pi^2\eta_j^2}{12} + \frac{\pi^4\eta_j^4}{360}\right)\frac{u^{*2}u_\beta}{\kappa}\right.$$

$$\left. + \frac{3}{16}\pi^4\eta_j^4\left(1 - \frac{2}{9}\pi^2\eta_j^2\right)\frac{u^* u_\beta^2}{\kappa} + \frac{\pi^6\eta_j^6}{48}u_\beta^3 + (U_e - u_\beta)\frac{u^{*2}}{\kappa^2}\right]$$

$$- (\gamma - 1)M_\infty^2\kappa^2 \frac{\rho_e}{\rho_\infty}\frac{u^{*2}}{\kappa^2}\left[\ln(\eta_j)(u_\beta - 2U_e)\frac{u^* u_\beta}{\kappa} + \ln^2(\eta_j)(U_e - u_\beta)\frac{u^{*2}}{\kappa^2}\right.$$

$$\left. + \frac{1}{3}\ln^3(\eta_j)\frac{u^{*3}}{\kappa^3} - \frac{1}{3}(U_e - u_\beta)(2U_e^2 + 2u_\beta U_e - u_\beta^2)\right] \tag{82}$$

In order to improve the behavior of the numerical solution near separation points, the quantities

$$\Delta a_{33} = -\frac{\frac{1}{64} + \left[\frac{3}{8}(I_1 - I_4) - \frac{1}{16}\right]\frac{a_{12}}{\kappa a_{11}}}{1 - 4I_1\frac{a_{12}}{\kappa a_{11}}}u_\beta^2 \tag{83}$$

and Δc_3 given in equation (51) are added to equations (76) and (78). The quantity c_3^* in the separated-flow solution is

$$c_3^* = \frac{64}{3\delta_s}\left(\frac{a_e}{a_\infty}\frac{c_3}{U_e^3}\right)_{u^*=0} \tag{84}$$

No other changes to the formulation are required.

APPROXIMATE POTENTIAL-FLOW METHOD

The transonic potential-flow method is the type presented by Murman and Cole in reference 15. The potential function is determined by solving finite-difference approximations to the governing equation at the grid points by successive line-overrelaxation techniques. In the present method a body-oriented, nonuniform Cartesian grid is used. A schematic representation of this computational grid is given in figure 2. The present method is unusual in that the exact nonlinear form of the airfoil boundary condition is used, but the boundary condition is applied on the airfoil chord line rather than the actual airfoil surface. This approximate nonlinear boundary condition has the advantage of the linear boundary condition of small-disturbance theory in that elaborate mappings of the airfoil are not required in order to apply the boundary condition at the surface, and yet it does not erroneously force the stagnation point to always be located at the airfoil leading edge. It should be noted that the stagnation point needs to be free to move back from the leading edge at the relatively large angles of attack at which trailing-edge separation occurs. The separation point is modeled in the potential-flow method as a free-streamline separation. Neumann boundary conditions are used on the attached-flow part of the airfoil and Dirchlet boundary conditions are used where the flow is separated. At present, the Dirchlet boundary conditions are constructed using either an approximate closed-form, separation-region solution or the well-founded empirical assumption that the pressure in the separation region is constant for nearly incompressible flows.

In the present potential-flow method various forms of the governing equation ranging from the full potential equation to the small-disturbance equation can be treated. In general, the governing equation can be written in the form

$$A\frac{\partial^2\phi}{\partial x^2} + B\frac{\partial^2\phi}{\partial x\,\partial z} + C\frac{\partial^2\phi}{\partial z^2} = 0 \tag{85}$$

where x and z are the coordinates in the chordwise and normal directions and ϕ is the perturbation velocity potential function. Very simple finite-difference expressions are used in the present method. The derivatives $\partial^2\phi/\partial x\,\partial z$ and $\partial^2\phi/\partial z^2$ are always approximated with central-difference expressions. The derivative $\partial^2\phi/\partial x^2$ is approximated with a central-difference expression if the coefficient A is positive and a backward-difference expression if A is negative. Shock waves can be treated either conservatively or nonconservatively. When the conservative approach is used, the derivative $\partial^2\phi/\partial x^2$ is approximated with the shock operator developed by Murman (ref. 16) and simplified by Barnwell (ref. 17).

It is well-known that the classical small-disturbance form of the governing equations lacks accuracy and that the full-potential equation is difficult to stabilize when the flow past the airfoil is critical and the procedure described in the previous paragraph is used. The difficulty with stabilization is due to the fact that the boundary conditions are not applied at the surface

and the fact that rotated differencing (ref. 18) is not used. However, a stable intermediate form has been found during the present investigation which yields the same results as the full-potential-equation form at nearly critical Mach numbers. This intermediate form is written with the following coefficients:

$$A = 1 - M_\infty^2 \left[\cos^2 \alpha + \left(\frac{\gamma + 1}{2} \right) \left(2 \frac{u}{v_\infty} \cos \alpha + \frac{u^2}{v_\infty^2} \right) \right] \tag{86}$$

$$B = -2M_\infty^2 \left(\cos \alpha + \frac{u}{v_\infty} \right) \left(\sin \alpha + \frac{w}{v_\infty} \right) \tag{87}$$

$$C = 1 - M_\infty^2 \sin^2 \alpha \tag{88}$$

where M_∞, α, and γ are the free-stream Mach number, angle of attack, and ratio of specific heats and where u and w are the velocity components in the x and z directions. For comparison, the coefficients A, B, and C for the classical small-disturbance equation are

$$A = 1 - M_\infty^2 + (\gamma + 1) M_\infty^2 \frac{u}{v_\infty} \tag{89}$$

$$B = 0 \tag{90}$$

$$C = 1 \tag{91}$$

For the full potential equation the coefficients are

$$A = 1 - M_\infty^2 \left[\cos^2 \alpha + \left(\frac{\gamma + 1}{2} \right) \left(\frac{2u}{v_\infty} \cos \alpha + \frac{u^2}{v_\infty^2} \right) + \left(\frac{\gamma - 1}{2} \right) \left(\frac{2w}{v_\infty} \sin \alpha + \frac{w^2}{v_\infty^2} \right) \right] \tag{92}$$

$$B = -2M_\infty^2 \left(\cos \alpha + \frac{u}{v_\infty} \right) \left(\sin \alpha + \frac{w}{v_\infty} \right) \tag{93}$$

$$C = 1 - M_\infty^2 \left[\sin^2 \alpha + \left(\frac{\gamma - 1}{2} \right) \left(\frac{2u}{v_\infty} \cos \alpha + \frac{u^2}{v_\infty^2} \right) + \left(\frac{\gamma + 1}{2} \right) \left(\frac{2w}{v_\infty} \sin \alpha + \frac{w^2}{v_\infty^2} \right) \right] \tag{94}$$

Note that in the present method (eqs. (86) to (88)), the dependence of A on w and the dependence of C on u and w have been ignored, and A, B, and C are correct as infinity is approached. A comparison between results of the present approximate potential method and those of the full potential method (ref. 18) is given in figure 3(a). Also shown are results calculated with the approximate method but with B = 0 (fig. 3(b)). It is clear from the results that the mixed derivative is an important contributor and should not be ignored.

The approximate Neumann boundary conditions for the attached-flow region of the airfoil surface for the present method and the full-potential-equation method are

$$\left.\frac{\partial \phi}{\partial z}\right|_{z=\pm 0} = \left[(v_\infty \cos \alpha + u)\left(\frac{dz_\pm}{dx} \pm \frac{d\delta^*}{dx}\right)\right]_{z=\pm 0} - v_\infty \sin \alpha \tag{95}$$

where $z = z_\pm(x)$ are the equations for the upper and lower airfoil surfaces. As indicated, these equations are exact in form but are evaluated along the airfoil chord line. For comparison, the boundary conditions for the classical small-disturbance equation are

$$\left.\frac{\partial \phi}{\partial z}\right|_{z=\pm 0} = v_\infty\left(\frac{dz_\pm}{dx} \pm \frac{d\delta^*}{dx}\right)_{z=\pm 0} \tag{96}$$

It should be noted that the present method and the full-potential-equation method both exhibit small-disturbance-like leading-edge singularity problems when grid points are located too near the leading edge. These problems occur because the boundary conditions are not applied at the airfoil surface.

In regions where the flow is separated, Dirchlet boundary conditions are used. One of the forms which is used in the present method is

$$\phi = \phi_s + \int_{s=x_s}^{s=x} (u_e - v_\infty \cos \alpha)\, ds \tag{97}$$

where ϕ_s and x_s are separation-point values and u_e is the boundary-layer edge velocity. The present boundary-layer method has a closed-form expression for u_e. Therefore, the integration in equation (97) is performed analytically.

The circulation on the airfoil is evaluated with a Kutta condition regardless of whether the flow at the trailing edge is attached or separated. This condition is applied in the form

$$u_{+,te} = u_{-,te} \tag{98}$$

which can be written as

$$\frac{\phi_+(x_{te} + \Delta x) - \phi_+(x_{te} - \Delta x)}{2\,\Delta x} = \frac{\phi_-(x_{te} + \Delta x) - \phi_-(x_{te} - \Delta x)}{2\,\Delta x} \tag{99}$$

where the subscript te denotes trailing-edge values. Equation (99) can be rewritten as

$$\Gamma = \phi_+(x_{te} - \Delta x) - \phi_-(x_{te} - \Delta x) \tag{100}$$

where Γ is the circulation. For attached flow the values of the perturbation velocity potential function in equation (100) are obtained by linear extrapolation, and for separated flow the values are obtained from equation (97).

The surface pressure coefficients are calculated from the following equation:

$$C_p = v + \frac{1}{4} M_\infty{}^2 v^2 + \frac{1}{24} M_\infty{}^4 v^3 \tag{101}$$

where

$$v = -\frac{u}{v_\infty}\left(2\cos\alpha + \frac{u}{v_\infty}\right) - \frac{w}{v_\infty}\left(2\sin\alpha + \frac{w}{v_\infty}\right) \tag{102}$$

This form is accurate at transonic speeds and is a determinate form for incompressible flow.

In the present method, the values of the perturbation velocity potential at the airfoil surfaces which are used to calculate the surface pressure coefficients are obtained with the following equation:

$$\phi_\pm(x) = \phi(x, \pm\Delta z) \pm \Delta z \frac{\partial \phi}{\partial z}(x, \pm 0) \tag{103}$$

where the derivatives $\partial\phi/\partial z$ are evaluated with equations (95). This form of extrapolation is also used for the full-potential-equation method. However, for the small-disturbance form the surface perturbation velocity potentials are

evaluated with linear extrapolation. (It is interesting to note that neither extrapolation procedure seems to work for the other form of the governing equation.)

The single-variable velocity-potential function φ, which is defined in equation (65) is related to the surface perturbation velocity potential function ϕ by the equation

$$\varphi = v_\infty x \cos \alpha + \phi \tag{104}$$

This equation is used to determine the separation-point value φ_s and the trailing-edge value φ_{te} which appear in equations (66) and (67). At the separation point ϕ is evaluated with equation (103) for both the present method and the full-potential-equation method and with linear extrapolation for the small-disturbance method. At the trailing edge ϕ is evaluated with linear extrapolation for all methods.

It should be noted that the incompressible limit of the present perturbation-velocity-potential method for separated flows was presented in reference 19. The advantages of the present method are its accuracy and the ease with which boundary conditions can be applied. The present method should be useful for accurately calculating flow past three-dimensional configurations, for which it is extremely difficult to enforce boundary conditions at wing surfaces.

RESULTS

Results computed with the present method for the lift curves of the NACA 0012 airfoil at free-stream Mach numbers of 0.15, 0.30, and 0.50 and Reynolds numbers of 2.0×10^6 and 6.0×10^6 are compared with experimental results in figure 4. Experimental results for free-stream Mach numbers of 0.15 and 0.30 were obtained in the Langley Low-Turbulence Pressure Tunnel (LTPT) by Charles L. Ladson (unpublished), and results for free-stream Mach numbers of 0.30 and 0.50 were obtained in the Langley 8-Foot Transonic Pressure Tunnel (8-Ft TPT) by Charles D. Harris (unpublished).

The results for the variation of the lift coefficient C_l with angle of attack at the lowest Mach number are essentially the same as results for incompressible flow. In the experiment, the boundary layer was tripped at points on the upper and lower surfaces $0.05c$ downstream of the leading edge. In the computation, the lower-surface boundary layer was tripped at $0.20c$ to avoid the numerical difficulties caused by starting the boundary layer ahead of the stagnation point, and the upper-surface boundary layer was again tripped at $0.05c$.

The first computations at a free-stream Mach number of 0.30 were made with the boundary layer tripped at the same points discussed previously. These results, which were in sharp contrast to the experimental results at this Mach number and which are not shown in the figure, were almost the same as the incompressible results. An examination of the pressure distributions revealed a

shock wave at 0.025c behind the leading edge on the upper surface for large angles of attack. Because this shock wave was located ahead of the upper-surface transition point, no shock-wave/boundary-layer interaction could occur. When the upper-surface transition point was moved to the leading edge, the results indicated by circular symbols, which are in excellent agreement with experimental results, were obtained. These results demonstrate that the decrease in maximum lift coefficient with increasing free-stream Mach number is due to a shock-wave/boundary-layer interaction. The computational results calculated with a linear form of the present method are represented by square symbols in figure 4. These results show that linear methods will not predict accurately the effect of Mach number on the maximum lift coefficient.

The results for a free-stream Mach number of 0.50 were calculated with the upper-surface transition point 0.05c behind the leading edge. These computations, which are in good agreement with experiment, were successful because the shock wave was located downstream of the transition point.

The pressure distribution for an NACA 0012 airfoil traveling at transonic speed is shown in figure 5. These results show a shock wave on the upper surface near the leading edge and separation at the trailing edge.

Sample calculations have been made with the alternate form of the present method, in which the mean kinetic-energy integral rather than the moment-of-momentum integral is used as the third equation. These calculations show there is no appreciable difference in the results of the two formulations.

CONCLUDING REMARKS

It has been demonstrated that potential-flow/boundary-layer methods can be used to calculate transonic flow past airfoils which are experiencing trailing-edge flow separation. Such methods can be used to determine the maximum lift coefficient and perhaps the effect of flap deflection on airfoil characteristics. Also, a transonic potential-flow method with easy-to-apply nonlinear boundary conditions has been developed. This method may be useful in calculating flow about winged configurations. Finally, a simple integral boundary-layer method for compressible turbulent flow with a two-level eddy viscosity model has been developed.

Langley Research Center
National Aeronautics and Space Administration
Hampton, VA 23665
April 23, 1981

REFERENCES

1. Jacob, Klaus: Berechnung der Abgelösten Inkompressiblen Strömung um Traflügelprofile und Bestimmung des Maximalen Auftriebs. Z. Flugwiss, Jahrg. 17, Heft 7, July 1969, pp. 221-230.

2. Bhateley, Ishwar C.; and MacWhirter, Jack W.: Development of Theoretical Method for Two-Dimensional Multi-Element Airfoil Analysis and Design. Part I: Viscous-Flow Analysis Method. AFFDL-TR-72-96, Part I, U.S. Air Force, Aug. 1972.

3. Geller, W.: Incompressible Flow Through Cascades With Separation. Boundary Layer Effects in Turbomachines, AGARD-AG-164, Dec. 1972, pp. 171-186.

4. Hendersen, M. L.: A Solution to the 2-D Separated Wake Modeling Problem and Its Use to Predict $C_{L,max}$ of Arbitrary Airfoil Sections. AIAA Paper 78-156, Jan. 1978.

5. Bristow, D. R.: Development of Panel Methods for Subsonic Analysis and Design. NASA CR-3234, 1980.

6. Carlson, Leland A.; and Rocholl, Bruce M.: Application of Direct-Inverse Techniques to Airfoil Analysis and Design. Advanced Technology Airfoil Research - Volume I, NASA CP-2045, Part 1, 1978, pp. 55-72.

7. Steger, Joseph L.: Implicit Finite-Difference Simulation of Flow About Arbitrary Two-Dimensional Geometries. AIAA J., vol. 16, no. 7, July 1978, pp. 679-686.

8. Kuhn, Gary D.; and Nielsen, Jack N.: Prediction of Turbulent Separated Boundary Layers. AIAA Paper No. 73-663, July 1973.

9. Nash, J. F.; and Hicks, J. G.: An Integral Method Including the Effect of Upstream History on the Turbulent Shear Stress. Computation of Turbulent Boundary Layers - 1968 AFOSR-IFP-Stanford Conference, Volume I - Methods, Predictions, Evaluation and Flow Structure, S. J. Kline, M. V,. Morkovin, G. Sovran, and D. J. Cockrell, eds., Stanford Univ., c.1969, pp. 37-45.

10. Cebeci, Tuncer; and Smith, A. M. O.: Analysis of Turbulent Boundary Layers. Academic Press, Inc., 1974.

11. Stewartson, K.: Correlated Incompressible and Compressible Boundary Layers. Proc. R. Soc. (London), Ser. A, vol. 200, no. A1060, Dec. 22, 1949, pp. 84-100.

12. Coles, Donald: The Law of the Wake in the Turbulent Boundary Layer. J. Fluid Mech., vol. 1, pt. 2, July 1956, pp. 191-226.

13. Klebanoff, P. S.: Characteristics of Turbulence in a Boundary Layer With Zero Pressure Gradient. NACA Rep. 1247, 1955. (Supercedes NACA TN 3178.)

14. White, Frank M.: Viscous Fluid Flow. McGraw-Hill, Inc., c.1974.

15. Murman, Earll M.; and Cole, Julian D.: Calculation of Plane Steady Transonic Flows. AIAA J., vol. 9, no. 1, Jan. 1971, pp. 114-121.

16. Murman, Earll M.: Analysis of Embedded Shock Waves Calculated by Relaxation Methods. AIAA J., vol. 12, no. 5, May 1974, p. 626-633.

17. Barnwell, Richard W.: Approximate Method for Calculating Transonic Flow About Lifting Wing-Body Configurations. NASA TR R-452, 1976.

18. Jameson, Antony: Iterative Solution of Transonic Flows Over Airfoils and Wings, Including Flow at Mach 1. Commun. Pure & Appl. Math., vol. XXVII, no. 3, May 1974, pp. 283-309.

19. Barnwell, Richard W.: Two Inviscid Computational Simulations of Separated Flow About Airfoils. AIAA Paper 76-379, July 1976.

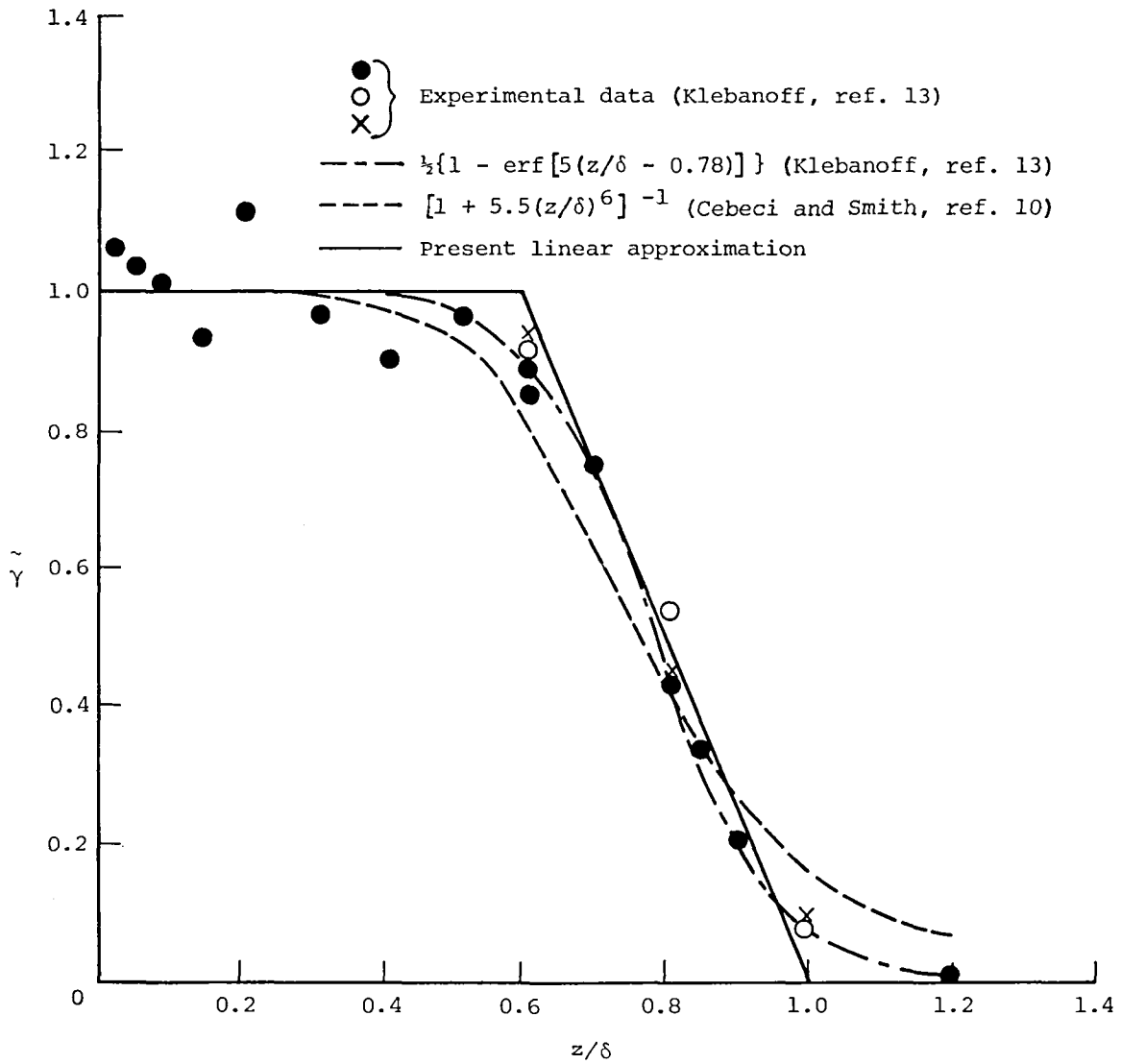

Figure 1.- Intermittency factor.

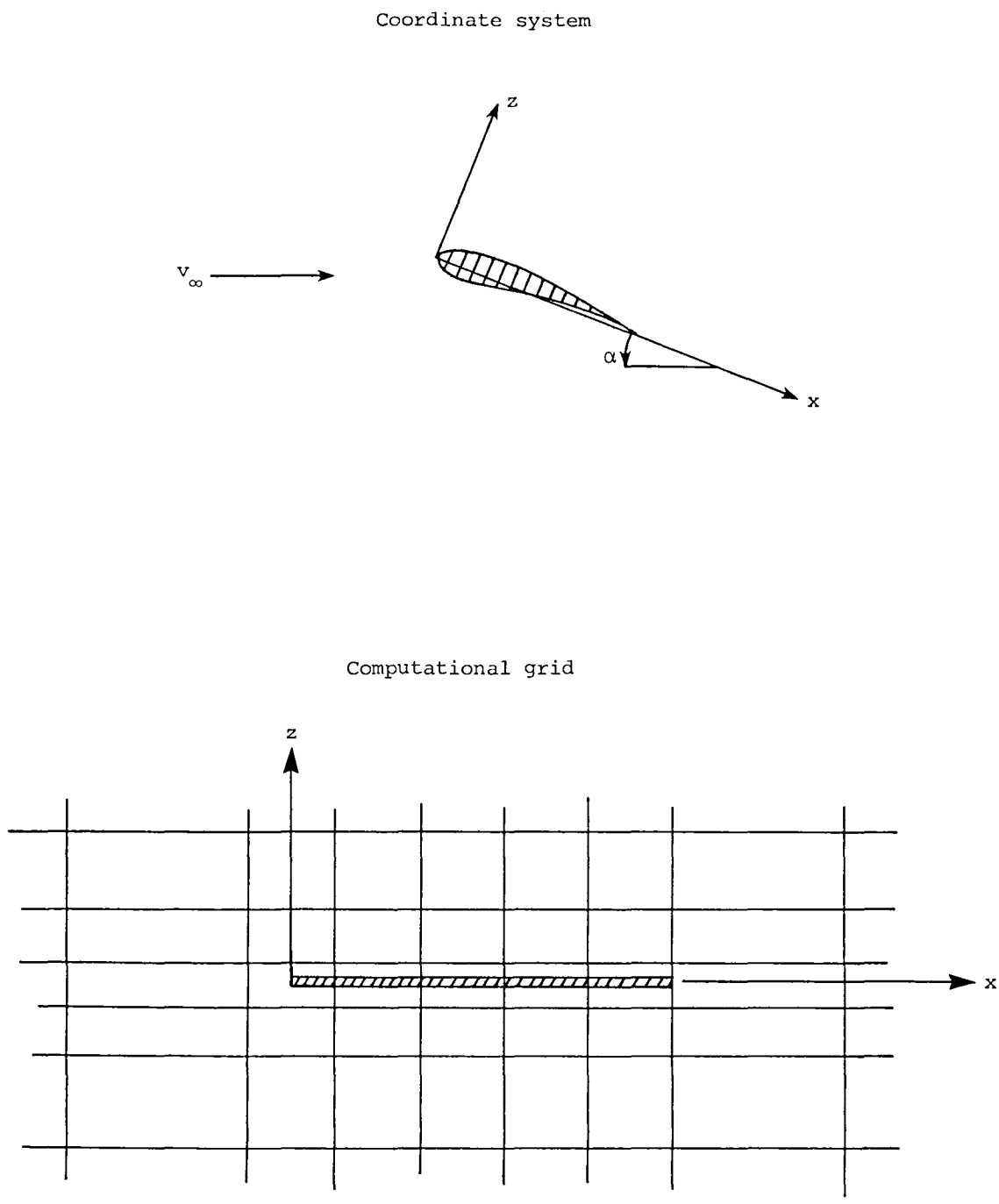

Figure 2.- Coordinate system and computational grid.

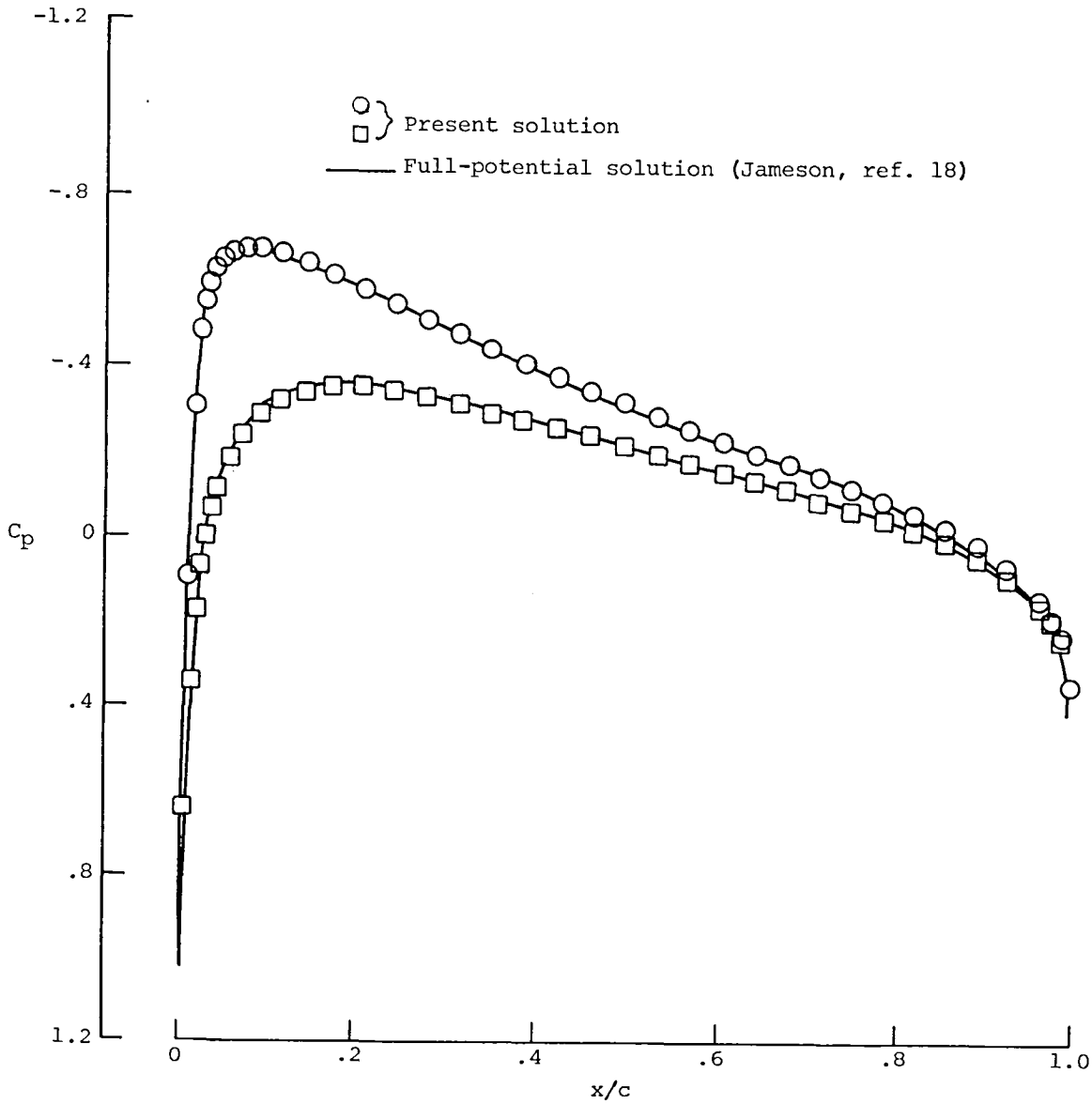

(a) Present solution.

Figure 3.- Comparison of inviscid solutions with full potential solution for NACA 0012 airfoil. $M_\infty = 0.50$; $\alpha = 1.00^\circ$.

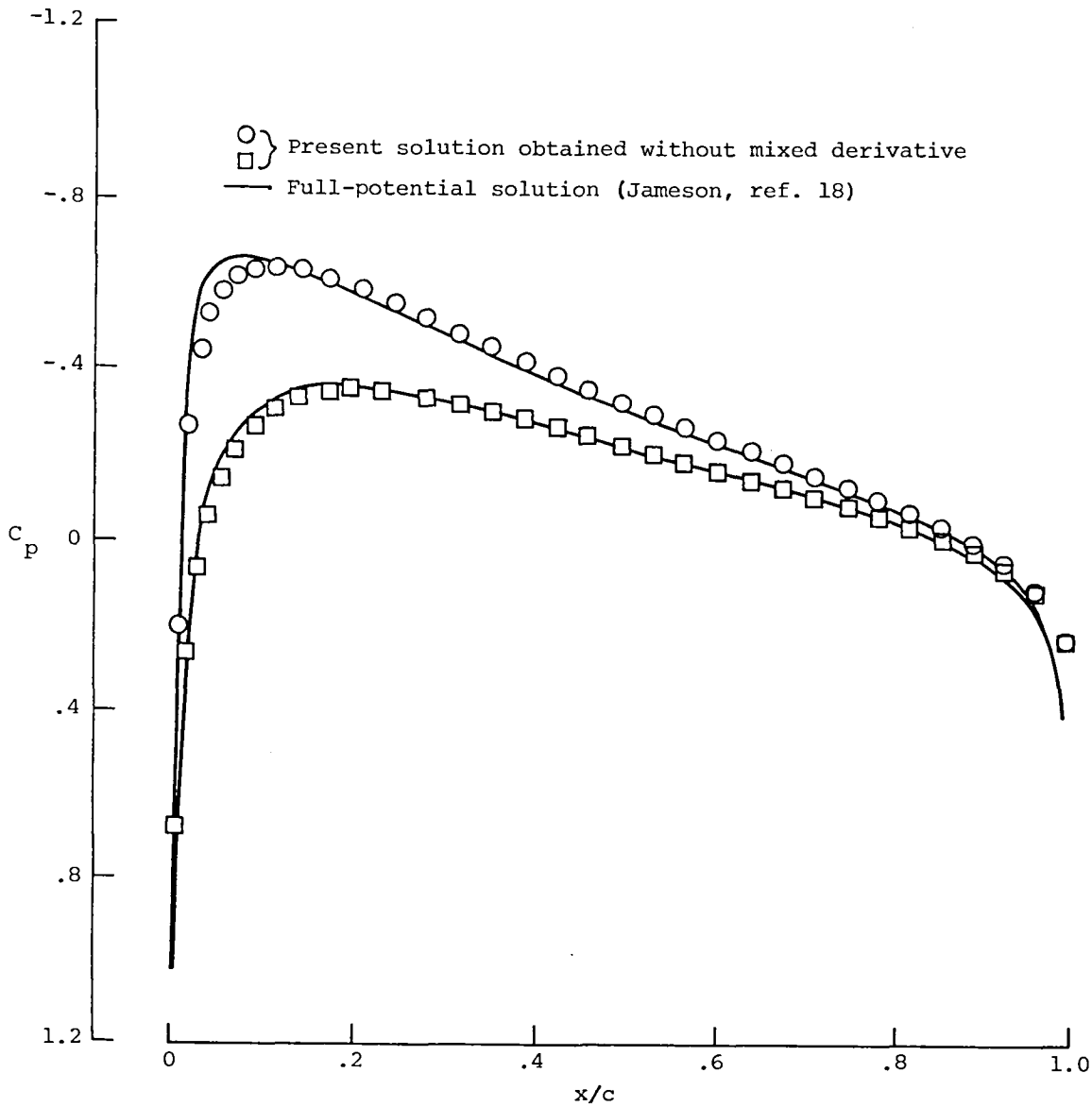

(b) Present solution obtained without mixed derivative.

Figure 3.- Concluded.

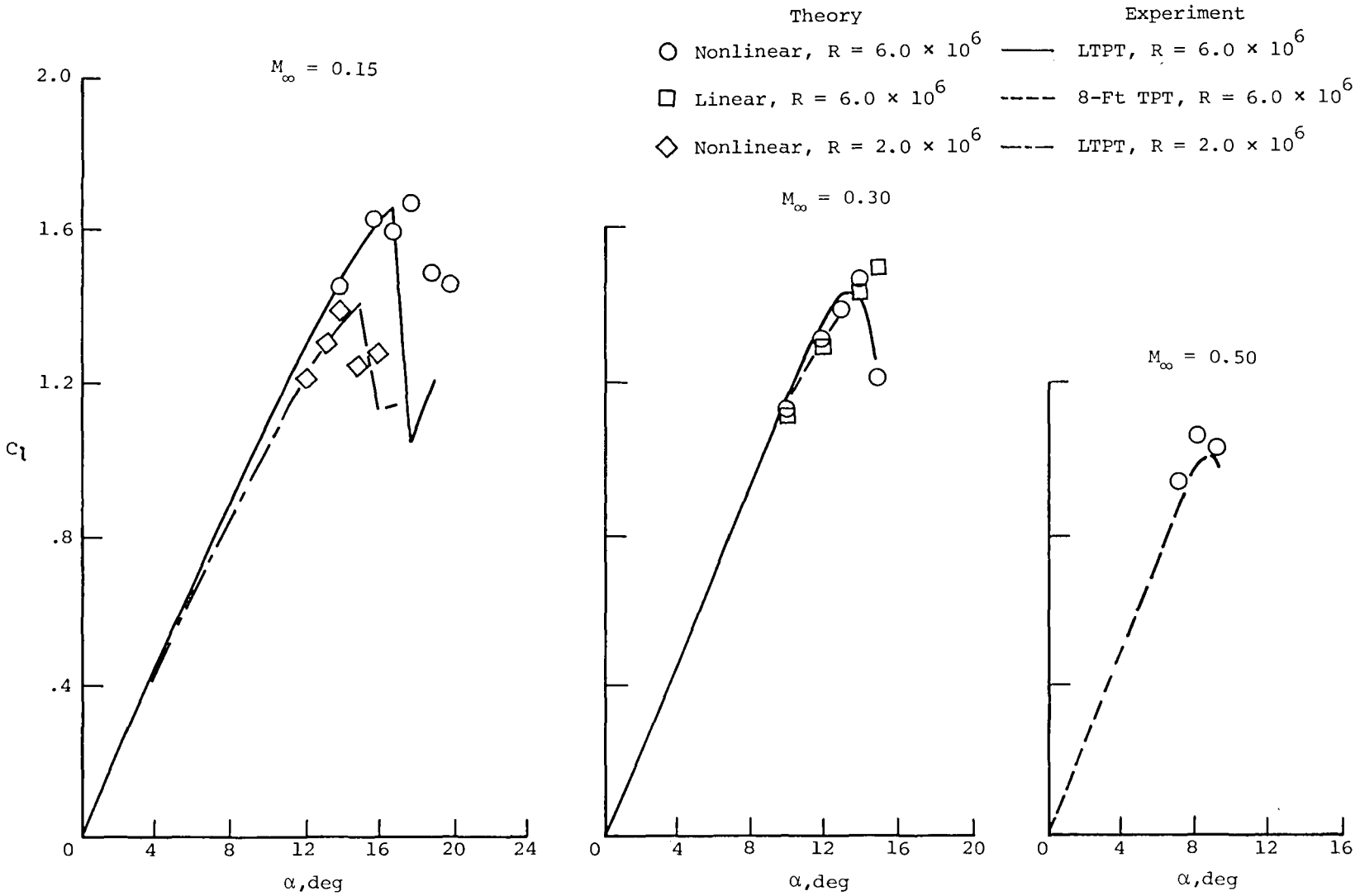

Figure 4.- Prediction of compressible trailing-edge separation effects for NACA 0012 airfoil.

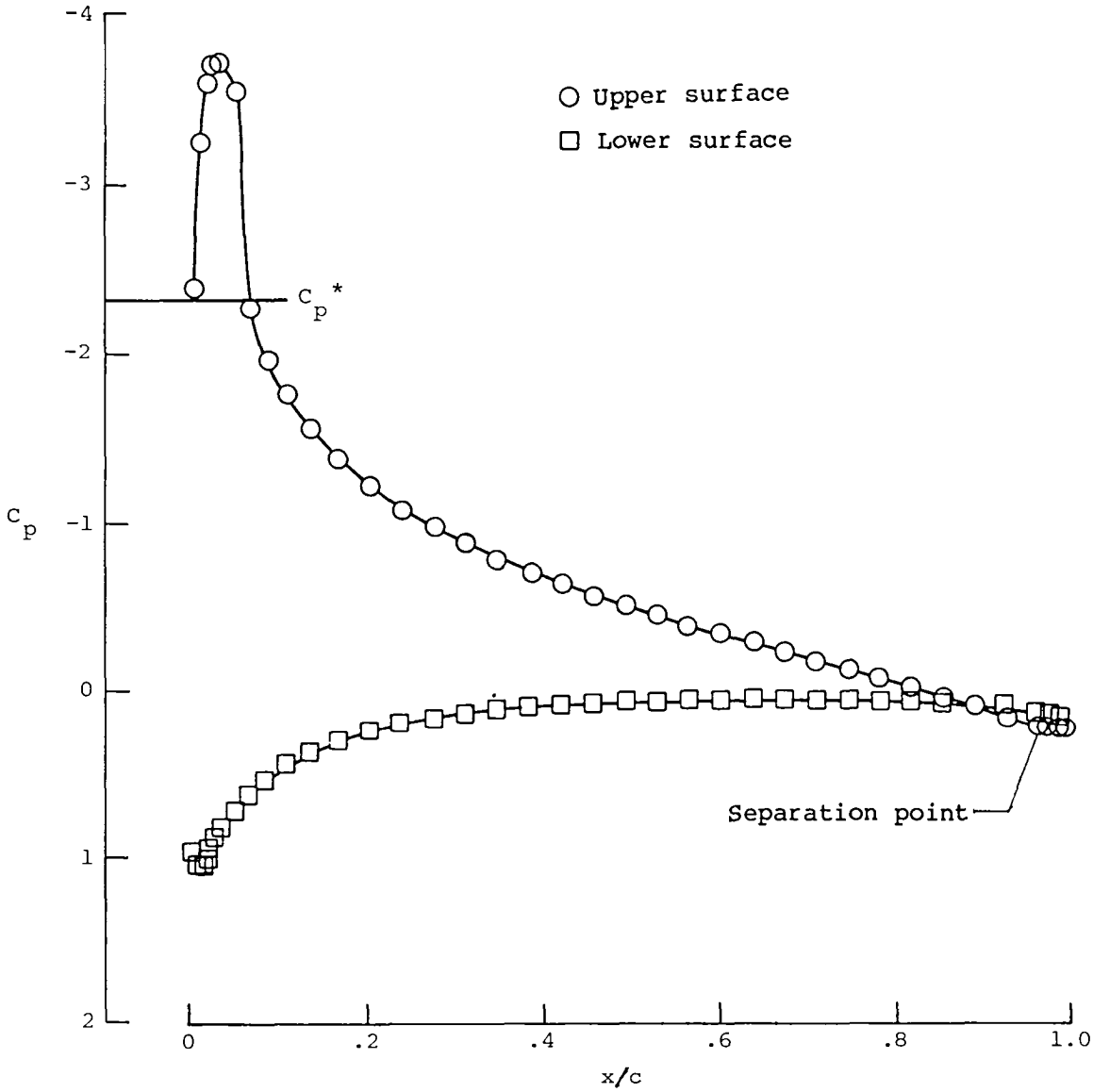

Figure 5.- Pressure distribution for transonic flow past NACA 0012 with trailing-edge separation. $M_\infty = 0.50$; $\alpha = 7.80^\circ$.

1. Report No.	2. Government Accession No.	3. Recipient's Catalog No.
NASA TM-81850		

4. Title and Subtitle	5. Report Date
A POTENTIAL-FLOW/BOUNDARY-LAYER METHOD FOR CALCULATING SUBSONIC AND TRANSONIC AIRFOIL FLOW WITH TRAILING-EDGE SEPARATION	June 1981
	6. Performing Organization Code: 505-31-33-05

7. Author(s)	8. Performing Organization Report No.
Richard W. Barnwell	L-14255
	10. Work Unit No.

9. Performing Organization Name and Address	11. Contract or Grant No.
NASA Langley Research Center Hampton, VA 23665	
	13. Type of Report and Period Covered: Technical Memorandum

12. Sponsoring Agency Name and Address	14. Sponsoring Agency Code
National Aeronautics and Space Administration Washington, DC 20546	

15. Supplementary Notes

16. Abstract

The development of a potential-flow/boundary-layer method for calculating subsonic and transonic turbulent flow past airfoils with trailing-edge separation is reported. A moment-of-momentum integral boundary-layer method is used which employs the law-of-the-wall/law-of-the-wake velocity profile and a two-layer eddy-viscosity model and ignores the laminar sublayer. All integrals across the boundary layer are obtained in closed form. Separation is assumed to occur when the shearing-stress velocity vanishes. A closed-form solution is derived for separated-flow regions where the shearing stress is negligible. In the potential-flow method, the exact form of the airfoil boundary condition is used, but it is applied at the chord line rather than the airfoil surface. This allows the accurate computation of flow about airfoils at large angles of attack but permits the use of body-oriented Cartesian computational grids. The governing equation for the perturbation velocity potential contains several terms in addition to the classical small-disturbance terms.

17. Key Words (Suggested by Author(s))	18. Distribution Statement
Turbulent boundary layer Separation Transonic flow Computational method	Unclassified - Unlimited Subject Category 02

19. Security Classif. (of this report)	20. Security Classif. (of this page)	21. No. of Pages	22. Price
Unclassified	Unclassified	37	A03

For sale by the National Technical Information Service, Springfield, Virginia 22161

NASA-Langley, 1981

National Aeronautics and
Space Administration

Washington, D.C.
20546

Official Business
Penalty for Private Use, $300

THIRD-CLASS BULK RATE

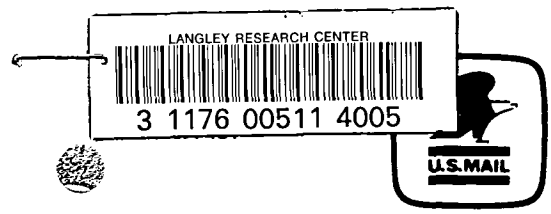

NASA

POSTMASTER: If Undeliverable (Section 158 Postal Manual) Do Not Return